

# DEPF: A UAV Multispectral Object Detector with Dual-Domain Enhancement and Priority-Guided Mamba Fusion

Shucong Li, Zhenyu Liu, Zijie Hong, Zhiheng Zhou, Xianghai Cao

## Abstract

Multispectral remote sensing object detection is one of the important application of unmanned aerial vehicle (UAV). However, it faces three challenges. Firstly, the low-light remote sensing images reduce the complementarity during multi-modality fusion. Secondly, the local small target modeling is interfered with redundant information in the fusion stage easily. Thirdly, due to the quadratic computational complexity, it is hard to apply the transformer-based methods on the UAV platform. To address these limitations, motivated by Mamba with linear complexity, a UAV multispectral object detector with dual-domain enhancement and priority-guided mamba fusion (DEPF) is proposed. Firstly, to enhance low-light remote sensing images, Dual-Domain Enhancement Module (DDE) is designed, which contains Cross-Scale Wavelet Mamba (CSWM) and Fourier Details Recovery block (FDR). CSWM applies cross-scale mamba scanning for the low-frequency components to enhance the global brightness of images, while FDR constructs spectrum recovery network to enhance the frequency spectra features for recovering the texture-details. Secondly, to enhance local target modeling and reduce the impact of redundant information during fusion, Priority-Guided Mamba Fusion Module (PGMF) is designed. PGMF introduces the concept of priority scanning, which starts from local targets features according to the priority scores obtained from modality difference. Experiments on DroneVehicle dataset and VEDAI dataset reports that, DEPF performs well on object detection, comparing with state-of-the-art methods. Our code is available in the supplementary material.

## Introduction

Unmanned aerial vehicles (UAV) play an important role in civil and public fields, including pest controlling, transportation monitoring and relief work etc. (Zhou et al. 2023) In addition, multispectral object detection is one of the most basic application of UAV, which depends on the remote sensing images provided by RGB camera and infrared imaging sensor. The RGB images contain color and texture-details about the real world, but their performance is limited by the low-light condition or overexposure. Instead, the infrared images provide stable capture of thermal data and target's outlines

Copyright © 2026, Association for the Advancement of Artificial Intelligence (www.aaai.org). All rights reserved.

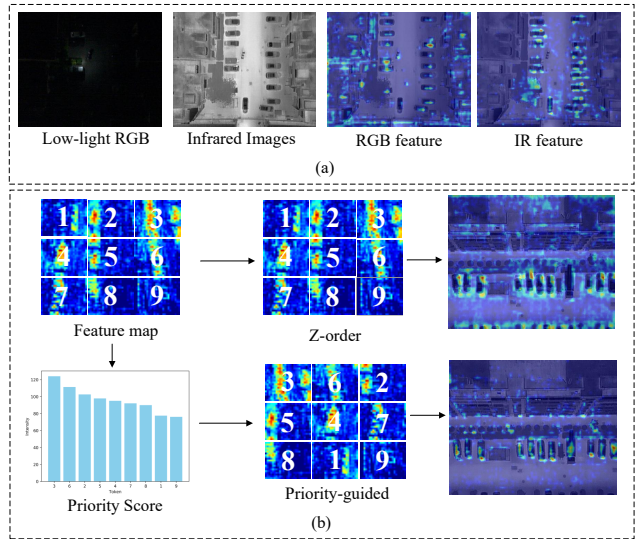


Figure 1: (a) The feature difference between low-light RGB images and infrared images. (b) The comparison between Z-order scanning and our Priority-guided scanning.

under any visual conditions, complementing the advantages offered by RGB images.

Therefore, many studies have focused on designing UAV-based multispectral object detection frameworks. According to the fusion mechanism, these methods could be categorized into pixel-wise fusion and feature-wise fusion.

The pixel-wise fusion retains most part of the nature details about the images. TarDAL (Liu et al. 2022) introduces generative adversarial network to reserve the common feature of two modalities in the fused images. SuperY-OLO (Zhang et al. 2023a) adopts input-level fusion of RGB and infrared images, enhancing feature representation by the super-resolution branch, while feature-wise fusion operates on multi-stage backbone features. To align fusion with downstream tasks, DetFusion (Sun et al. 2022a) guides training through detection loss derived from fused images.

Different from pixel-wise fusion, the feature-wise fusion enhance the performance of detectors by leveraging the complementarity of multi-modality features. Halfway Fusion (Liu et al. 2016) is the first work that proposes feature-

wise fusion for multispectral pedestrian detection. Later, (Sun et al. 2022b) designs UA-CMDet and a novel RGB-Infrared drone dataset named DroneVehicle. However, UA-CMDet adopts simple feature concatenation to achieve multispectral fusion. (Zhang et al. 2022) introduces complementary image and discriminative feature fusion to make full use of the effective information between the two modalities and filter out redundant features. To address inaccurate cross-modal fusion, C<sup>2</sup>Former (Yuan and Wei 2024) employs CNNs for feature extraction, while utilizes a Transformer-based Inter-modality Cross-Attention module to generate aligned and complementary features. Inspired by the linear complexity of Mamba, DMM (Zhou et al. 2025b) designs disparity-guided mamba fusion to adaptively merge features and achieve lightweight object detection.

However, the above methods also face three challenges: 1) Although the infrared images provide supplementary information about the scenarios. The low-light RGB images reduces the complementarity during multi-modality fusion, as the obvious differences in their feature maps. As shown in Figure 1 (a). 2) In the fusion stage, the local small target modeling are interfered with redundant information. Specially, as shown in Figure 1 (b), the Mamba-based fusion methods like DMM adopts Z-order scanning focuses on global modeling and suppresses the local dependencies of 2D images. Therefore, the feature map contains noise. 3) The transformer-based methods like C<sup>2</sup>Former has large computational costs for detection task.

To address these challenges, a UAV Multispectral Object Detector with Dual-domain Enhancement and Priority-guided Mamba Fusion named DEPF is proposed. Firstly, to enhance low-light remote sensing RGB images, DDE Module is designed, which contains CSWM block and FDR block. Specially, CSWM block contains Cross-Scale Mamba Scanning for the low-frequency (LF) components from 2D discrete wavelet transform (2D-DWT) to enhance the global brightness of images. FDR block constructs Spectrum Recovery Network (SRN) to enhance the frequency spectra features to recover the texture-details. Secondly, PGMF Module is designed to enhance the local target modeling for multispectral fusion. PGMF constructs Priority Score Network (PSN) to obtain the priorities of tokens from feature differences. The priority scores guide serialization to prioritize tokens containing local target features.

Overall, our contributions could be summarized as follow:

- DEPF is proposed to enhance the low-light RGB images and improve complementarity in the fusion stage, as well as enhance the local target modeling and achieve feature alignment during fusion.
- DDE is designed and contains CSWM and FDR block. CSWM block improves the global brightness and FDR block recovers the texture-details of low-light RGB images.
- PGMF module is designed to focus on local target modeling, reducing the interference of redundant information. To our best knowledge, PGMF is the first approach to improve Mamba mechanism for multi-modality fusion.
- The experiment results on DroneVehicle dataset and

VEDAI dataset show that DEPF performs well on object detection and achieves lightweight computation.

## Related Work

**Multispectral Object Detection** The multispectral usually includes visible and infrared images, both of which could provide complementary information under unstable lighting conditions for object detection. Existing multispectral fusion mechanism could be classified into pixel-wise fusion and feature-wise fusion.

Pixel-wise fusion aggregates two spectral data into a whole images ahead of schedule, and feeds the images to the detector. (Cao et al. 2023) proposes a local-global adaptive dynamic learning method to fuse multi-modal data. To ensure the fusion network is task-optimized, DetFusion (Sun et al. 2022a) employs the detection loss computed from the fused images as guidance during training. Employing input-level fusion of RGB and IR images. Feature-wise fusion focuses on the features from different stages of backbone network. These stage features are fused and fed to the detection head. TSFADet (Yuan, Wang, and Wei 2022) designs an alignment module to predict modality deviations with subsequent feature map calibration. (Zhao et al. 2024) propose a coarse-to-fine framework to remove redundant information and select features for fusion dynamically. To resolve modality calibration and fusion inaccuracies, C<sup>2</sup>Former (Yuan and Wei 2024) introduced an inter-modal cross-attention module, while its Adaptive Feature Sampling module mitigated computational costs from global attention.

However, these works focuses on the scenarios under normal lighting conditions, ignoring the application on the low-light scenarios. Moreover, they lack the attention to reduce the impact of redundant information for local small target detection.

**Low-light Images Enhancement** There are many frameworks having been designed for enhancing the low-light images, which lacks enough texture-details due to under exposed characteristic. Brightness enhancement in FourLLIE (Feng et al. 2022) is achieved by dual-stage estimation of amplitude transformation maps within the frequency domain. DiffLL (Jiang et al. 2023) implements sequential denoising refinements in diffusion models to generate realistic details for low-light image enhancement task, highlighting their practical viability. (Zhou et al. 2025a) proposes a framework with guidance of generative perceptual priors obtained from vision-language models, it shows good generalization on real-world data. WaveMamba (Zou et al. 2024) combines wavelet transformation and Mamba mechanism to achieve low-light images restoration. These works enhance the texture-details of instances in low-light images, which gives important help to the detection task.

**Vision Mamba** Mamba (Gu and Dao 2023) mechanism has been paid attention to computer vision field because it can model long-distance dependencies and maintain linear computational complexity. Many vision mamba works has developed and performed well in the vision researches. The

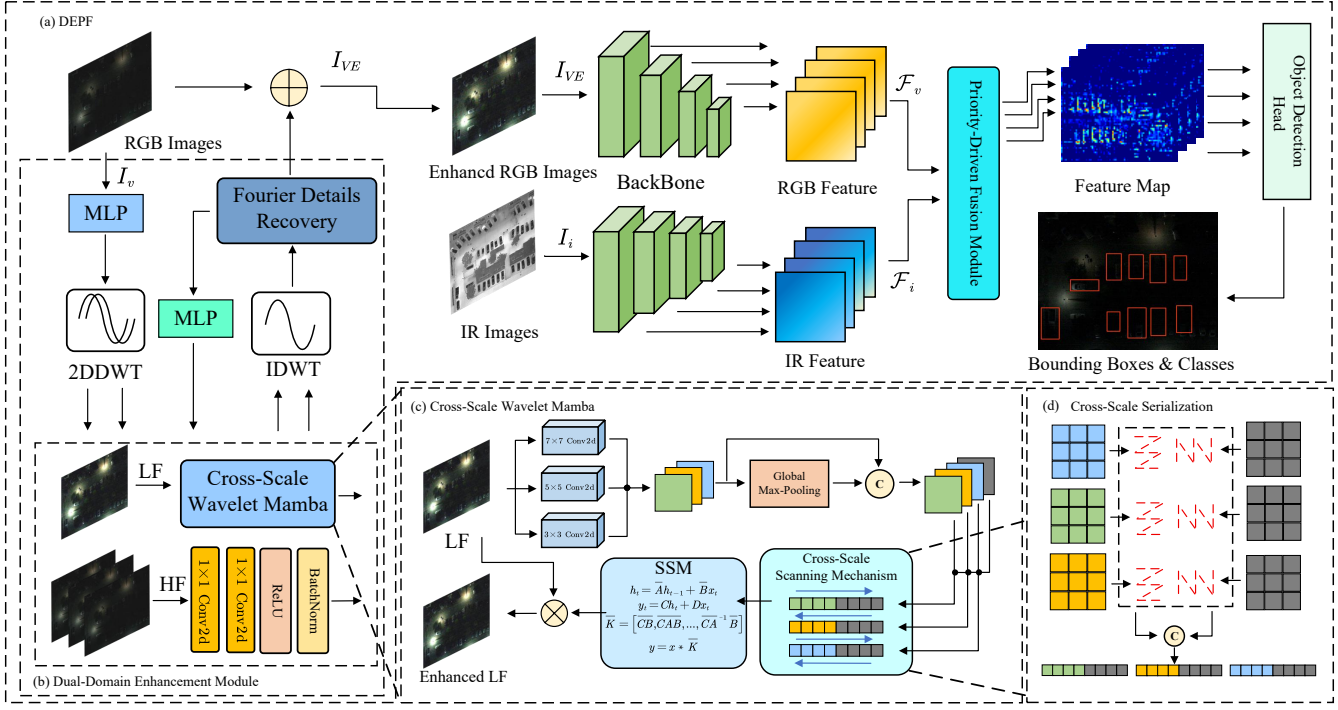


Figure 2: The overall architecture of DEPF. (a) is the pipeline of DEPF, (b) is the architecture of DDE module, while (c) is the processing of CSWM block including the Cross-Scale Scanning Mechanism. (d) shows the Cross-Scale Serialization in the CSWM block.

visual state-space model VMamba (Liu et al. 2024) preserves SSM’s global receptive field capability but operates at linear computational cost, enabling order-of-magnitude speed gains. Vim (Zhu et al. 2024) proposes a new vision backbone with bidirectional scanning mamba, This architecture embeds positional cues into sequences while compacting representations through bidirectional state-space compression. Vision mamba is widely adopted for images classification tasks, like SpectralMamba (Yao et al. 2024), S<sup>2</sup>Mamba (Wang et al. 2025) etc., and images segmentation tasks like RS<sup>3</sup>Mamba (Ma, Zhang, and Pun 2024), VM-Unet (Ruan, Li, and Xiang 2024) etc. These works could achieve good performance with low computation complexity.

However, most of vision mamba works adopts Z-order serialization for scanning the images, which focuses on global context and suppresses the local dependencies. Therefore, for the remote sensing images with many small objects, the background information brings degradation to local targets modeling in the multi-modality fusion stage under the Z-order serialization.

## Method

### Dual-Domain Mamba Enhancement Module

The low-frequency component in wavelet-domain contains most of information about low-light RGB images, while the high-frequency component only contains small parts of texture-details (Zou et al. 2024). Therefore, the low-frequency component could be adopted to enhance the over-

all brightness of images. For the texture-details, it is worth noting that frequency domain has good global modeling capability. The amplitude spectrum contains the energy of details while the phase spectrum contains the structure of the instances in the images. Therefore, these two spectra could be adopted to recover the texture details of images.

Following the above ideas, DDE module is designed for enhancing the low-light RGB remote sensing images, which is shown in Fig.1. DDE module consists of two parts, the first part is CSWM block, which is designed for low-frequency component enhancement. The second part is FDR block, which is designed to enhance the texture details of images.

**Cross-Scale Wavelet Mamba Block** For the low-light RGB remote sensing images  $I_v \in \mathbb{R}^{B \times C \times H \times W}$ , they are decomposed by the N-level Haar wavelet, yielding low-frequency components  $LL$  and high-frequency components  $[HL, LH, HH]_n$ :

$$LL, [HL, LH, HH]_n, \dots, [HL, LH, HH]_1 = DWT(I_v) \quad (1)$$

The  $LL$  is enhanced by CSWM block, which is designed by adopting the strong context-aware properties of Mamba (Albert Gu and Tri Dao, 2023). To ensure that the local objects dependencies are enhanced,  $LL$  is conveyed to three convolution layers with kernel sizes  $i \in [3, 5, 7]$  to obtain multi-scale feature and global feature:

$$f_i = DWConv(LL, i) \quad \forall i \in \{3, 5, 7\} \quad (2)$$

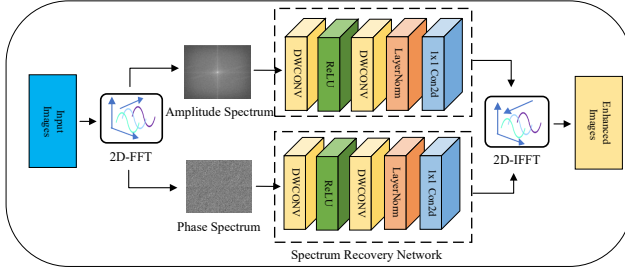


Figure 3: The processing of FDR block. It enhances the amplitude and phase features by spectrum recovery network.

$$f_g = GAP(f_3, f_5, f_7) \quad (3)$$

where  $DWConv()$  denotes depthwise convolution,  $GAP()$  denotes global average pooling operator.

For learning the context information, the Cross-Scale Scanning Mechanism is designed. Concretely, every scale feature  $f_i$  and the global feature  $f_g$  are flatten and concatenated together so that the relative scale information could be learned. To adequately exploit the latent features, the forward scanning and backward scanning are set up simultaneously. Therefore, the cross-scale scanning sequences could be described as:

$$f_{cross}^i = flatten(f_i) + flatten(f_g) \quad (4)$$

$$f_{seq}^i = f_{cross}^i + \overline{f_{cross}^i} \quad \forall i \in \{3, 5, 7\} \quad (5)$$

where  $flatten()$  denotes flattening operator and  $\overline{f_{cross}^i}$  denotes the reverse sequence of  $f_{cross}^i$ . After the SSM module  $SSM()$ , the enhanced  $LL$  is obtained by:

$$LL_e = LL \times \sum_i SSM(f_{seq}^i) \quad \forall i \in \{3, 5, 7\} \quad (6)$$

The high-frequency components are passed through MLP and join in wavelet reconstruction together with  $LL_e$ :

$$I_{ve}^n = IDWT(LL_e, [HL, LH, HH]_n) \quad \forall n \in [0, N] \cap \mathbb{Z} \quad (7)$$

**Fourier Details Recovery** The enhanced images  $I_{ve}^n$  also lacks texture-details after low-frequency enhancement. Therefore,  $I_{ve}^n$  is conveyed to FDE module for recovering most of texture-details. FDE contains spectrum recovery networks which could enhance the details of amplitude spectrum (AS) and phase spectrum (PS) obtained by 2D-FFT. The enhanced MS and PS are then transformed into time-domain to obtain rich texture-details images  $I_{VE}$ . This process could be described as:

$$\begin{aligned} AS &= \text{abs}(FFT(I_{ve}^n)) \\ PS &= \arctan\left(\frac{\text{imag}(FFT(I_{ve}^n))}{\text{real}(FFT(I_{ve}^n))}\right) \\ AS_e &= SRN(AS) \\ PS_e &= SRN(PS) \\ I_{VE} &= IFFT(AS_e, PS_e) \end{aligned} \quad (8)$$

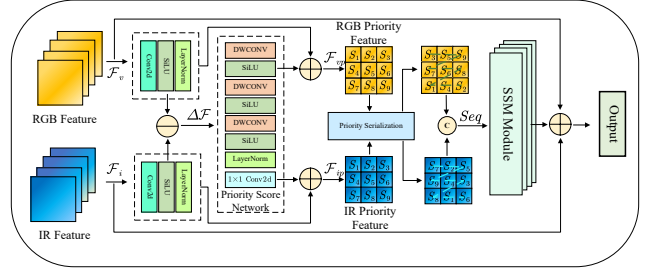


Figure 4: The overall architecture of PGMF module. The modalities features are transformed into sequences following the priority scores of tokens, which is obtained from Priority Score Network.

where  $SRN()$  denotes the spectrum recovery network, which consists of two  $DWConv$  layers, one  $ReLU$  layer, one  $LayerNorm$  layer and one  $Linear$  layer.  $I_{VE}$  should be conveyed to CSWM block if it is not in the last level of 2D-DWT.

### Priority-Guided Mamba Fusion Module

For the feature maps of remote sensing images, there is an obvious difference in the proportion of local target features and background features. However, the Z-order serialization focuses on global modeling, which brings redundant information to weaken the local targets modeling. Therefore, if the scanning prioritizes the feature of local targets, not only does the impact of redundant information be lessened, but also the original global feature is retained. The fused feature map with obvious targets details could be obtained by scanning the priority sequences of two modalities. In the appendix file, we conduct theoretical proof about the advantage of Priority-guided for Mamba modeling.

Following the above ideas, Priority-Guided Mamba Fusion Module (PGMF) is designed to achieve high effective RGB-IR feature fusion, which is shown in Figure 4.

The input feature  $\mathcal{F}_v$  and  $\mathcal{F}_i$  are conveyed to small MLPs to reflect into latent space. Moreover, it is worth noting that not only does the feature difference  $\Delta\mathcal{F}$  contain location information of the targets, but also show the regions that be focused mistakenly. Therefore,  $\Delta\mathcal{F}$  is conveyed to Priority Score Network to align feature difference and obtain priority matrices  $PMat$ . Both of two modalities could obtain their priority features by adding with  $PMat$ :

$$\begin{aligned} \Delta\mathcal{F} &= \mathcal{F}_{vl} - \mathcal{F}_{il} \\ PMat &= PSN(\Delta\mathcal{F}) \\ \mathcal{F}_{vp} &= \mathcal{F}_{vl} + PMat \\ \mathcal{F}_{ip} &= \mathcal{F}_{il} + PMat \end{aligned} \quad (9)$$

where  $\mathcal{F}_{vl}$  and  $\mathcal{F}_{il}$  denote the latent representations of RGB feature map and IR feature map.  $PSN()$  denotes the Priority Score Network, which consists of three  $DWConv$ - $SiLU$  layers, one  $LayerNorm$  layer and one  $Linear$  layer.

The serialization sets up to obtain the sequences by following the descent priority scores, which separates the target from interference information. Therefore, the scanning

starts from the targets and ends up with the background information. Due to the difference of two modality, the priority orders of them may not consistent.

$$\begin{aligned} Seq_v &= Ser(F_{vl}, argSort(F_{vp})) \\ Seq_i &= Ser(F_{il}, argSort(F_{ip})) \\ Seq &= Seq_v + Seq_i \end{aligned} \quad (10)$$

Where  $Ser()$  denotes serialization operator and  $argSort()$  denotes obtaining the tokens after sorting.

Two sequences are fused together and conveyed to SSM module. the input features of two modalities are added with priority feature by residual connection:

$$\begin{aligned} \mathcal{F}_p &= SSM(Seq) \\ \mathcal{F}_{fus} &= \mathcal{F}_p + \mathcal{F}_v + \mathcal{F}_i \end{aligned} \quad (11)$$

The pseudocode and performance analysis of PGMF module could be seen in the appendix file of the supplementary materials.

## Loss Function

The loss function of DEPF follows conventional object detection loss and classification loss. Therefore, the cross-entropy loss function (C. E. Shannon, 1948) is adopted for the optimizing of object detection task, while the Smooth L1 loss function (Ross Girshick, 2015) is adopted for the optimizing of regression task. Therefore, the loss function of DEPF could be described as:

$$\mathcal{L} = \alpha \mathcal{L}_{det} + \beta \mathcal{L}_{reg} \quad (12)$$

where  $\alpha$  and  $\beta$  denote the weights of loss item. During training phase, they are set to  $\{1.0, 1.0\}$ .

## Experiment

### Datasets and Metrics

DEPF is evaluated on DroneVehicle (Sun et al., 2022) and VEDAI (Sebastien Razakarivony and Frederic Jurie, 2016) benchmarks.

**DroneVehicle Dataset** The DroneVehicle dataset is a large RGB-Infrared remote sensing dataset obtained by the real time flying of drones. The scenarios includes parking lots, roads, residential areas and etc. in daylight and nighttime. It contains 28,439 pairs of RGB and IR images with five classes of instances, including cars, trucks, freight cars, vans and buses. All of the classes have 95,3087 annotated bboxes and labels. The images are sized at  $840 \times 712$  pixels with an additional 100 pixels white border and the actual size is  $640 \times 512$  pixels.

**VEDAI Dataset** VEDAI dataset provides 1,246 paired RGB and infrared aerial images with sizes of  $1024 \times 1024$  or  $512 \times 512$  pixels for vehicle detection in varied urban/rural environments. Its oriented annotations cover 9 categories: core vehicle types such as cars, trucks, vans etc. and auxiliary objects such as airplanes, boats etc.

**Metrics** The metrics we choose is mean Average Precision (mAP) which includes mAP@0.5 and mAP@0.5:0.95. mAP@0.5 represents that predicted bounding box is regarded as correct if the Intersection over Union (IoU) with the ground truth is at least 0.5. mAP@0.5:0.95 is the mean value of mAP under different IoU thresholds, whose range is from 0.5 to 0.95 with step size 0.05.

### Implementation Details

DEPF is built on MMdetection and MMrotate platform. All of the experiments are conducted on four NVIDIA RTX 3090 GPUs with 24GB of memory. The environment of training and testing is Pytorch 2.1.2 and CUDA 11.8. DEPF is trained with 12 epochs and batch size of 4. The AdamW optimizer is adopted with an initial learning rate of 0.0001 and a weight decay of 0.05. We adopt Vision-Mamba as our backbone network and S<sup>2</sup>ANet as our detection head. The sizes of input images are  $512 \times 640$  for DroneVehicle dataset and  $512 \times 512$  for VEDAI dataset respectively. For the settings of CSWM block, Haar is chosen as wavelet basis, and the level of 2D-DWT is set to 2.

### Comparing with SOTA Methods

**Comparison Results on the DroneVehicle dataset** Table 1 shows the comparison results on the DroneVehicle dataset. Our DEPF is compared with single-modality methods and multi-modality methods respectively. It could be observed that DEPF has significant performance in terms of mAP@0.5 and mAP@0.5:0.95.

Concretely, for single RGB modality methods, RoITransformer (Ding et al. 2019) achieves best performance with mAP@0.5 of 61.6% and mAP@0.5:0.95 of 32.9%, which is surpassed by our DEPF by 17.3 points and 18.3 points respectively. Moreover, DEPF achieves obvious performance for the category detection, such as the result on Car with mAP@0.5 of 90.5% and Bus with mAP@0.5 of 90.0%. For single infrared modality methods, all of the detectors perform better than adopting RGB modality only due to the harmful effects of low-light RGB images. DEPF achieves best performance with mAP@0.5 of 78.9%, while surpassed by DTNet (Zhang et al. 2024) with mAP@0.5:0.95 of 52.9%. However, DEPF outperforms DTNet most in category detection, such as 3.7 points gains on Truck. DEPF also surpasses some of multispectral detectors. Comparing with C<sup>2</sup>Former (Yuan and Wei 2024), it obtains 4.7 points improvement with mAP@0.5 and 3.7 points improvement with mAP@0.5:0.95. Comparing with TarDAL, it obtains 7.3 points improvement with mAP@0.5 and 8.1 points improvement with mAP@0.5:0.95.

Figure 5 shows the visualization results on the Drone Vehicle dataset. DEPF is compared with C<sup>2</sup>Former and DMM in the low-light scenarios, as the regions marked by blue circles show. In the first scene, C<sup>2</sup>Former detects a bus-stop as car and bus. DMM doesn't have such false detection but it classifies the freight-car as car. By contrast, our DEPF avoids these mistakes. In the second scene, it could be observed that DEPF makes correct classification of a car at night. In the third scenarios, C<sup>2</sup>Former and DMM make false detection

Methods	Modality	Car	Truck	Freight Car	Bus	Van	mAP@0.5	mAP@0.5:0.95
RetinaNet	RGB	78.5	34.4	24.1	69.8	28.8	25.0	23.4
R <sup>3</sup> Det	RGB	80.3	56.1	42.7	80.2	44.4	27.4	27.4
KFIoU	RGB	76.3	50.0	33.2	78.2	35.7	54.7	28.0
RoITransformer	RGB	61.6	55.1	42.3	85.5	44.8	61.6	32.9
YOLOV5	RGB	76.2	48.9	35.5	68.9	40.4	54.0	30.2
Oriented R-CNN	RGB	80.1	53.8	41.6	85.4	43.3	60.8	32.7
PKINet-S	RGB	76.4	53.0	40.8	79.1	45.7	59.0	31.2
Ours	RGB+Infrared	<b>90.5</b>	<b>79.4</b>	<b>66.6</b>	<b>90.0</b>	<b>67.8</b>	<b>78.9</b>	<b>51.2</b>
RetinaNet	Infrared	88.8	35.4	39.5	76.5	32.1	54.5	30.4
R <sup>3</sup> Det	Infrared	89.5	48.3	16.6	87.1	39.9	62.3	36.7
S <sup>2</sup> ANet	Infrared	89.9	54.5	55.8	88.9	48.4	67.5	40.4
KFIoU	Infrared	90.2	65.0	48.5	89.0	43.0	67.1	41.2
ReDet	Infrared	89.8	53.9	43.3	84.8	33.2	61.0	36.2
GWD	Infrared	89.8	39.6	26.5	75.0	23.2	50.8	30.7
PKINet-S	Infrared	90.2	67.3	56.3	88.8	51.2	70.8	43.8
DTNet	Infrared	90.2	65.7	<b>78.1</b>	89.2	<b>67.9</b>	78.2	<b>52.9</b>
Ours	RGB+Infrared	<b>90.5</b>	<b>79.4</b>	66.6	<b>90.0</b>	67.8	<b>78.9</b>	51.2
UA-CMDet	RGB+Infrared	87.5	60.7	46.8	87.1	38.0	64.0	40.1
Halfway-Fusion	RGB+Infrared	90.1	62.3	58.5	89.1	49.8	70.0	42.9
GLFNet	RGB+Infrared	90.3	72.7	53.6	88.0	52.6	71.4	42.9
AR-CNN	RGB+Infrared	90.1	64.8	62.1	89.4	51.5	71.6	—
MBNet	RGB+Infrared	90.1	64.4	62.4	88.8	53.6	71.9	—
TSFADet	RGB+Infrared	89.9	67.9	63.7	89.8	54.0	73.1	—
CIAN	RGB+Infrared	90.1	63.8	60.7	89.1	50.3	70.8	—
C <sup>2</sup> Former	RGB+Infrared	90.2	68.3	64.4	89.8	58.5	74.2	47.5
TarDAL	RGB+Infrared	89.5	68.3	56.1	89.4	59.3	72.6	43.3
DMM	RGB+Infrared	90.4	78.9	66.2	89.5	<b>68.3</b>	78.6	50.6
Ours	RGB+Infrared	<b>90.5</b>	<b>79.4</b>	<b>66.6</b>	<b>90.0</b>	67.8	<b>78.9</b>	<b>51.2</b>

Table 1: Comparative experiment results on the DroneVehicle dataset. ‘-’ represents that the result is not reported.

Methods	Car	Truck	Boat	Van	Others	mAP@0.5
RetinaNet	48.9	16.8	4.4	5.9	14.1	18.0
YOLO-S	<b>95.5</b>	65.5	74.2	70.7	47.9	70.8
YOLOV3	91.3	51.1	65.2	62.6	30.7	60.2
ROITransfomer	77.3	56.1	56.7	60.2	42.8	58.6
DAGN	81.3	32.9	41.5	<b>78.5</b>	53.9	57.6
Faster-RCNN	71.6	49.1	35.6	57.0	29.5	48.6
S <sup>2</sup> ANet	73.0	39.2	13.9	32.3	23.1	36.3
C <sup>2</sup> Former	76.7	52.0	43.3	48.0	41.9	52.4
CMAFF	81.7	58.8	66.0	68.5	51.5	65.3
DMM	84.2	65.7	72.3	72.5	56.2	70.2
Ours	85.3	<b>66.7</b>	<b>74.3</b>	73.0	<b>56.4</b>	<b>71.1</b>

Table 2: Comparative experiment results on the VEDAI dataset, the best results are marked with bold font.

that regards oval flower beds as cars at night, while DEPF avoids this mistake. These results shows that our method achieve robustness detection and classification in the low-light scenarios.

**Comparison Results on the VEDAI dataset** Table 2 shows the comparison results on the VEDAI dataset. It could be observed that DEPF outperforms many of detectors with mAP@0.5 of 71.1%. However, for the Car and Van, DEPF is surpassed by YOLO-S (Betti and Tucci 2023) with 95.5% and DAGN (Zhang et al. 2019b) with 78.5%. These two de-

Methods	Input Size	Para (MB) ↓	FLOPs (G) ↓	FPS (img/s) ↑
TSFADet		104.7	109.8	<b>19</b>
C <sup>2</sup> Former		118.5	115.6	11
DMM	512 × 640	88.1	108.8	17
Ours		<b>80.3</b>	<b>108.3</b>	16

Table 3: The complexity comparison between our DEPF and SOTA on NVIDIA RTX 3090 GPU.

tectors only adopts RGB images to achieve object detection, they are be impacted by the redundant information from multi-modality fusion mechanism. Nevertheless, DEPF also surpasses them on Truck, Boat and Other categories. Comparing with challenging DMM (Zhou et al. 2025b), DEPF obtains 0.9 points improvement with mAP@0.5 and obtains most 2 points improvement with mAP@0.5 on Boat in terms of specific categories.

**Comparison of Computational Complexity** Table 3 shows the comparison results of computational complexity between DEPF and SOTA methods. Notably, this experiment is conducted on a NVIDIA RTX 3090 GPU, and the size of test input tensor is 512 × 640 with batch size of 1. It could be observed that our method has 80.3 MB parameter count and 108.3 GFLOPs (Giga Floating-Point Operations Per second). Especially, comparing C<sup>2</sup>Former, it reduces about 32.2% parameter count and 6.3% GFLOPs. Compar-

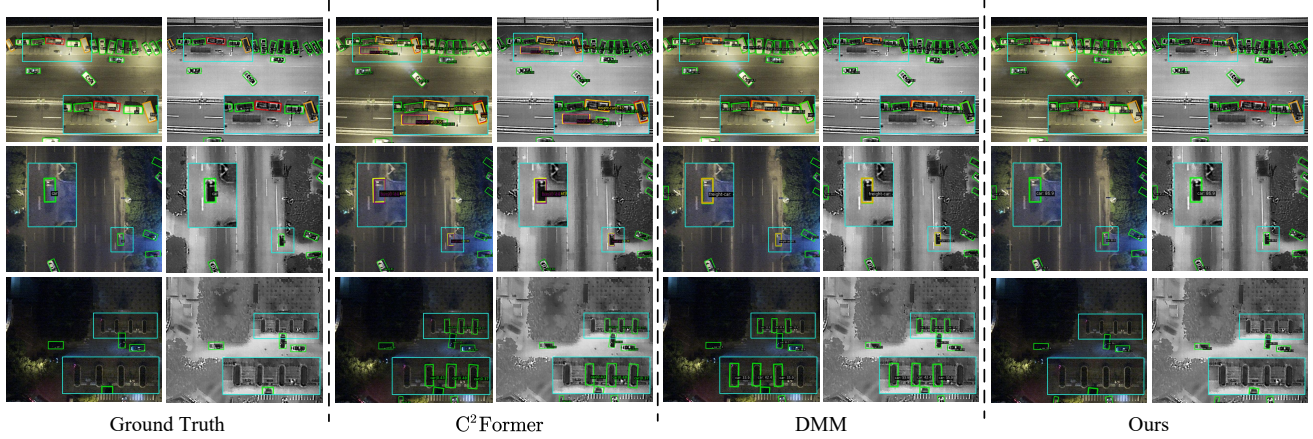


Figure 5: The visual comparison results on the DroneVehicle datasets. The advantages of our method are marked with blue circles. DEPF overcomes incorrect classification, missed detections, and false detections in the low-light scenarios.

Models	DDE		Fusion		mAP	
	CSWM	FDR	Z-order	PGMF	0.5	0.5:0.95
model 1			✓		77.8	49.7
model 2				✓	78.1	50.8
model 3	✓		✓		77.8	50.0
model 4		✓	✓		75.4	49.1
model 5	✓	✓	✓		78.3	50.7
model 6	✓	✓		✓	<b>78.9</b>	<b>51.2</b>

Table 4: Ablation study on the designed module on the DroneVehicle dataset.

ing with DMM, it only reduces 7.8 MB parameter count and 0.5 GFLOPs. However, DEPF has no advantage in terms of FPS. The inference speed of TSFANet is the highest with 19 img/s, while DEPF’s is 16 img/s, which is also lower than DMM. The reason of this result is that the the inference speed is slowed down by 2D-DWT and FFT in DDE module, they don’t have parameter count but has computational costs.

## Ablation Study

**Ablation Study on the Designed Modules** The ablation study about the designed modules is conducted and the result is shown in Table 4. Comparing model 1 and model 2, the mAP@0.5 and mAP@0.5:0.95 improve about 0.3 points and 1.1 points when Z-order fusion is replaced with PGMF module, which demonstrates that the priority scanning could achieve more effective fusion than Z-order scanning. Comparing model 3, model 4 and model 5, it could be seen that introducing CSWM and FDR block only could not improve the metrics. In contrast, he mAP@0.5 and mAP@0.5:0.95 improve about 0.5 points and 1 points when both of them are introduced. This result demonstrates that enhancing the brightness and recovering the texture-details are important for detection. After adding PGMF module, the metrics improve to the optimum, which demonstrates that priority

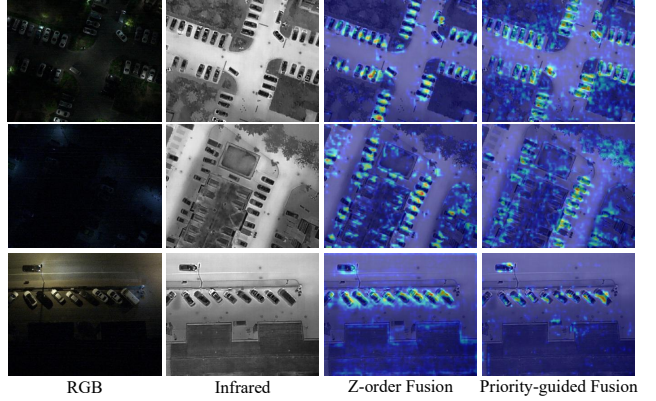


Figure 6: Comparison result about the Z-order Fusion and Priority-guided Fusion on the feature maps.

scanning fusion with enhanced images feature could achieve more correct detection.

**Visualization of fusion feature maps** To evaluate our priority scanning, the visualization of fusion feature maps are shown in Figure 6. It could be observed that the degree of focus is located on background easily under Z-order fusion mechanism. By contrast, our priority scanning fusion shifts the focus of attention to the instances, suppressing the interference from background information.

**Other Experiments** We add other experiment results in the appendix file of the supplementary materials.

## Conclusion

In this article, DEPF is proposed with DDE module and PGMF module. DDE contains CSWM and FDR block to enhance the global brightness and recover texture-details of low-light RGB images. PGMF introduces Priority Scanning to enhance the local target modeling and achieve feature

alignment. To our best knowledge, PGMF is the first approach to improve Mamba mechanism for multi-modality fusion. The experiment results shows that DEPF performs well on object detection and achieves lightweight computation.

## References

Betti, A.; and Tucci, M. 2023. YOLO-S: a lightweight and accurate YOLO-like network for small target detection in aerial imagery. *Sensors*, 23(4): 1865.

Cai, X.; Lai, Q.; Wang, Y.; Wang, W.; Sun, Z.; and Yao, Y. 2024. Poly kernel inception network for remote sensing detection. In *Proceedings of the IEEE/CVF conference on computer vision and pattern recognition*, 27706–27716.

Cao, B.; Sun, Y.; Zhu, P.; and Hu, Q. 2023. Multi-modal gated mixture of local-to-global experts for dynamic image fusion. In *Proceedings of the IEEE/CVF international conference on computer vision*, 23555–23564.

Ding, J.; Xue, N.; Long, Y.; Xia, G.-S.; and Lu, Q. 2019. Learning ROI transformer for oriented object detection in aerial images. In *Proceedings of the IEEE/CVF conference on computer vision and pattern recognition*, 2849–2858.

Feng, H.; Wang, L.; Wang, Y.; and Huang, H. 2022. Learnability enhancement for low-light raw denoising: Where paired real data meets noise modeling. In *Proceedings of the 30th ACM International Conference on Multimedia*, 1436–1444.

Gu, A.; and Dao, T. 2023. Mamba: Linear-time sequence modeling with selective state spaces. *arXiv preprint arXiv:2312.00752*.

Han, J.; Ding, J.; Xue, N.; and Xia, G.-S. 2021. Redet: A rotation-equivariant detector for aerial object detection. In *Proceedings of the IEEE/CVF conference on computer vision and pattern recognition*, 2786–2795.

Jiang, H.; Luo, A.; Fan, H.; Han, S.; and Liu, S. 2023. Low-light image enhancement with wavelet-based diffusion models. *ACM Transactions on Graphics (TOG)*, 42(6): 1–14.

Liu, J.; Fan, X.; Huang, Z.; Wu, G.; Liu, R.; Zhong, W.; and Luo, Z. 2022. Target-aware dual adversarial learning and a multi-scenario multi-modality benchmark to fuse infrared and visible for object detection. In *Proceedings of the IEEE/CVF conference on computer vision and pattern recognition*, 5802–5811.

Liu, J.; Zhang, S.; Wang, S.; and Metaxas, D. N. 2016. Multispectral deep neural networks for pedestrian detection. *arXiv preprint arXiv:1611.02644*.

Liu, Y.; Tian, Y.; Zhao, Y.; Yu, H.; Xie, L.; Wang, Y.; Ye, Q.; Jiao, J.; and Liu, Y. 2024. Vmamba: Visual state space model. *Advances in neural information processing systems*, 37: 103031–103063.

Ma, X.; Zhang, X.; and Pun, M.-O. 2024. Rs 3 mamba: Visual state space model for remote sensing image semantic segmentation. *IEEE Geoscience and Remote Sensing Letters*, 21: 1–5.

Qingyun, F.; and Zhaokui, W. 2022. Cross-modality attentive feature fusion for object detection in multispectral remote sensing imagery. *Pattern Recognition*, 130: 108786.

Ruan, J.; Li, J.; and Xiang, S. 2024. Vm-unet: Vision mamba unet for medical image segmentation. *arXiv preprint arXiv:2402.02491*.

Sun, Y.; Cao, B.; Zhu, P.; and Hu, Q. 2022a. Dtfusion: A detection-driven infrared and visible image fusion network. In *Proceedings of the 32nd ACM International Conference on Multimedia*, 4003–4011.

Sun, Y.; Cao, B.; Zhu, P.; and Hu, Q. 2022b. Drone-based RGB-infrared cross-modality vehicle detection via uncertainty-aware learning. *IEEE Transactions on Circuits and Systems for Video Technology*, 32(10): 6700–6713.

Wang, G.; Zhang, X.; Peng, Z.; Zhang, T.; and Jiao, L. 2025. S 2 mamba: A spatial-spectral state space model for hyperspectral image classification. *IEEE Transactions on Geoscience and Remote Sensing*.

Yang, X.; Yan, J.; Feng, Z.; and He, T. 2021a. R3det: Refined single-stage detector with feature refinement for rotating object. In *Proceedings of the AAAI conference on artificial intelligence*, volume 35, 3163–3171.

Yang, X.; Yan, J.; Ming, Q.; Wang, W.; Zhang, X.; and Tian, Q. 2021b. Rethinking rotated object detection with gaussian wasserstein distance loss. In *International conference on machine learning*, 11830–11841. PMLR.

Yang, X.; Zhou, Y.; Zhang, G.; Yang, J.; Wang, W.; Yan, J.; Zhang, X.; and Tian, Q. 2022. The KFIoU loss for rotated object detection. *arXiv preprint arXiv:2201.12558*.

Yao, J.; Hong, D.; Li, C.; and Chanussot, J. 2024. Spectral-mamba: Efficient mamba for hyperspectral image classification. *arXiv preprint arXiv:2404.08489*.

Yuan, M.; Wang, Y.; and Wei, X. 2022. Translation, scale and rotation: Cross-modal alignment meets RGB-infrared vehicle detection. In *European Conference on Computer Vision*, 509–525. Springer.

Yuan, M.; and Wei, X. 2024. C<sup>2</sup>former: Calibrated and complementary transformer for rgb-infrared object detection. *IEEE Transactions on Geoscience and Remote Sensing*, 62: 1–12.

Zhang, J.; Lei, J.; Xie, W.; Fang, Z.; Li, Y.; and Du, Q. 2023a. SuperYOLO: Super resolution assisted object detection in multimodal remote sensing imagery. *IEEE Transactions on Geoscience and Remote Sensing*, 61: 1–15.

Zhang, L.; Liu, Z.; Zhang, S.; Yang, X.; Qiao, H.; Huang, K.; and Hussain, A. 2019a. Cross-modality interactive attention network for multispectral pedestrian detection. *Information Fusion*, 50: 20–29.

Zhang, L.; Liu, Z.; Zhu, X.; Song, Z.; Yang, X.; Lei, Z.; and Qiao, H. 2021. Weakly aligned feature fusion for multimodal object detection. *IEEE Transactions on Neural Networks and Learning Systems*.

Zhang, N.; Liu, Y.; Liu, H.; Tian, T.; Ma, J.; and Tian, J. 2024. DTNet: A specialized dual-tuning network for infrared vehicle detection in aerial images. *IEEE Transactions on Geoscience and Remote Sensing*, 62: 1–15.

Zhang, N.; Liu, Y.; Liu, H.; Tian, T.; and Tian, J. 2023b. Oriented infrared vehicle detection in aerial images via mining frequency and semantic information. *IEEE Transactions on Geoscience and Remote Sensing*, 61: 1–15.

Zhang, P.; Zhao, J.; Wang, D.; Lu, H.; and Ruan, X. 2022. Visible-thermal UAV tracking: A large-scale benchmark and new baseline. In *Proceedings of the IEEE/CVF Conference on Computer Vision and Pattern Recognition*, 8886–8895.

Zhang, Z.; Liu, Y.; Liu, T.; Lin, Z.; and Wang, S. 2019b. DAGN: A real-time UAV remote sensing image vehicle detection framework. *IEEE Geoscience and Remote Sensing Letters*, 17(11): 1884–1888.

Zhao, T.; Yuan, M.; Jiang, F.; Wang, N.; and Wei, X. 2024. Removal then selection: A coarse-to-fine fusion perspective for RGB-infrared object detection. *arXiv e-prints*, arXiv-2401.

Zhou, H.; Dong, W.; Liu, X.; Zhang, Y.; Zhai, G.; and Chen, J. 2025a. Low-light image enhancement via generative perceptual priors. In *Proceedings of the AAAI Conference on Artificial Intelligence*, volume 39, 10752–10760.

Zhou, K.; Chen, L.; and Cao, X. 2020. Improving multispectral pedestrian detection by addressing modality imbalance problems. In *European conference on computer vision*, 787–803. Springer.

Zhou, M.; Li, T.; Qiao, C.; Xie, D.; Wang, G.; Ruan, N.; Mei, L.; Yang, Y.; and Shen, H. T. 2025b. Dmm: Disparity-guided multispectral mamba for oriented object detection in remote sensing. *IEEE Transactions on Geoscience and Remote Sensing*.

Zhou, T.; Chen, J.; Shi, Y.; Jiang, K.; Yang, M.; and Yang, D. 2023. Bridging the view disparity between radar and camera features for multi-modal fusion 3d object detection. *IEEE Transactions on Intelligent Vehicles*, 8(2): 1523–1535.

Zhu, L.; Liao, B.; Zhang, Q.; Wang, X.; Liu, W.; and Wang, X. 2024. Vision mamba: Efficient visual representation learning with bidirectional state space model. *arXiv preprint arXiv:2401.09417*.

Zou, W.; Gao, H.; Yang, W.; and Liu, T. 2024. Wave-mamba: Wavelet state space model for ultra-high-definition low-light image enhancement. In *Proceedings of the 32nd ACM International Conference on Multimedia*, 1534–1543.